

Phase-Separation-Induced Gelation of Poly(9,9-dioctylfluorene)/Methylcyclohexane Solution

Chun-Yu Chen,[†] Chih-Shun Chang,^{‡,§} Siao-Wun Huang,[‡] Jean-Hong Chen,^{*,‡}
Hsin-Lung Chen,^{*,†} Ching-Iuan Su,[§] and Show-An Chen[†]

[†]Department of Chemical Engineering, National Tsing Hua University, Hsin-Chu 30013, Taiwan,

[‡]Department of Polymer Materials, Kun Shan University, Tainan Hsien 71003, Taiwan, and [§]Department of Polymer Engineering, National Taiwan University of Science and Technology, Taipei 10672, Taiwan

Received February 10, 2010; Revised Manuscript Received March 18, 2010

ABSTRACT: The gelation behavior of the solution of a conjugated polymer, poly(9,9-dioctylfluorene) (PF8), with a poor solvent, methylcyclohexane (MCH), induced by aging at room temperature has been investigated. Light scattering and optical microscopy revealed that the gelation was driven by a macrophase separation occurred through a spinodal decomposition mechanism. Although the spinodal decomposition could proceed to the late stage, the interconnected morphology was arrested to give rise to the gel property of the system. The phase-separated gel was composed of an isotropic phase and a PF8-enriched liquid crystalline phase. The liquid crystalline phase was further found to consist of sheetlike aggregates (as revealed by small-angle X-ray scattering) in which a fraction of the PF8 chains formed the β -phase (as disclosed by the optical spectra) which dominated the photoluminescence spectrum of the gel. The PF8/MCH gel could be disintegrated by moderate heating to ca. 70 °C. This gel-to-sol transition was accompanied by the disruptions of the sheetlike aggregates and the β -phase which led to homogenization of the solution.

Introduction

Conjugated polymers are the main active materials used in organic photonic and optoelectronic devices such as photodiodes, light-emitting diodes,¹ photovoltaics,² and thin-film transistors.³ The potential of conjugated polymers in these applications stems from their unique semiconducting properties and the ease of solution processing. Their solubility in common organic solvents is usually accomplished by grafting flexible short side chains to the rigid conjugated segments to perturb the interchain $\pi-\pi$ interaction.

The intrinsic chain stiffness coupled with the amphiphilic nature (due to solubility difference between the backbone and the side chain) and $\pi-\pi$ interaction make the solution behavior of conjugated polymers highly complex. Conjugated polymer chains are seldom completely dispersed in solution even at large dilution (e.g., below the overlap concentration). Abundant experimental studies have demonstrated the existence of submicrometer or micrometer aggregates in the solutions, and their presence drastically modifies the photophysical properties of the system.^{4,5} Network and disk (sheet) are two types of structural entity identified for the aggregates based on recent small-angle X-ray and neutron scattering studies.^{6–9} The internal structure (e.g., chain packing) of the aggregates has however not been addressed unequivocally.

The structure of conjugated polymer solution also exhibits strong time dependence due to the slow dynamics to attain equilibrium or metastable equilibrium state upon polymer dissolution (usually assisted by mechanical stirring and heating). Such a time dependence is sometimes manifested by slow gelation, where the initially viscous liquid solution transforms into gel upon prolonged aging at ambient or subambient

temperatures.^{10–13} This gelation phenomenon is prevalent among different types of conjugated polymers (e.g., poly(phenylene ethynylene)s,¹⁰ poly(phenylenevinylene)s,¹¹ polyfluorenes,¹² and polythiophenes¹³), but the underlying mechanism and gel structure may vary from system to system.

We have been interested in the gelation behavior of the solutions of a conjugated polymer, poly(9,9-dioctylfluorene) (PF8).¹² PF8 is a structural archetype of polyfluorenes which have been considered as the most promising conjugated polymer for application in blue-light-emitting devices.¹⁴ The dispersion states of PF8 in an aromatic solvent, toluene, and its hydrogenated counterpart, methylcyclohexane (MCH), have been studied recently by small-angle neutron scattering (SANS). Toluene is a better solvent than MCH because its aromatic moiety may interact favorably with PF8 through $\pi-\pi$ interaction.⁹ Knaapila et al. revealed that PF8 could be dissolved down to the molecular level in dilute (0.5–1.0 wt %) toluene solutions where they remained as stiff rods.⁹ We have shown that PF8 chains aggregated to form networks containing domains of aligned segments in the semidilute toluene solution.¹⁵ In MCH the majority of PF8 chains were found to form bilayered sheetlike aggregates. The formation of these aggregates was often accompanied by the appearance of a mesomorphic β -phase in which the PF8 chains adopt the C_β conformation. The C_β conformer is characterized by the carbon–carbon torsional angles between the repeating units of $\pm 160^\circ$, and this makes the backbone more planar to self-assemble into lamellar structure (β -structure).¹⁶ The β -phase was found to display very narrow line widths in adsorption, prompt and delayed fluorescence, phosphorescence, and photoinduced triplet absorption.¹⁷

The solutions of PF8 with cyclohexane, tetrahydrofuran, and toluene have been reported to undergo gelation upon prolonged storage at room temperature and –20 °C.^{12,18} The gelation of toluene solution was found to be driven by a macrophase separation, where in the course of phase separation the regions

*To whom correspondence should be addressed. E-mail: hlchen@che.nthu.edu.tw (H.-L.C.); kelvenc@mail.ksu.edu.tw (J.-H.C.).

enrich of PF8 gradually developed the sheetlike aggregates in which a fraction of the chains adopted C_β conformation to form the β -phase.^{9,12} Theoretically, a phase separation leading to the nematic–isotropic coexistence region has been predicted by a mean-field model by Knaapila et al.¹⁹ In this model, a membrane phase (relevant to the sheetlike aggregates observed experimentally) in which the PF chains packed to form bilayered sheets was predicted to exist over a narrow temperature range, while the nematic–isotropic coexistence was found to dominate the phase diagram in the phase-separated region. However, the membrane structure may be kinetically arrested due to slow phase separation. Hence, PF8 may form three structural entities, namely, free chains, loose membrane, and β -domains in the poorer solvent.¹⁹

In this paper, we report a systematic investigation of the gelation behavior of PF8/MCH solution induced by room-temperature aging over a relatively broad concentration range. Because of the poorer solvent quality of MCH, this solution system undergoes gelation much more easily than toluene solution in the sense that the gels can be formed at lower concentration (e.g., 0.1 wt %) and higher temperature (e.g., room temperature) over a relatively short aging time. Here we attempt to resolve the structure and gelation mechanism by dynamic light scattering (DLS), small-angle X-ray scattering (SAXS), optical microscopy, and optical spectra measurements. The effect of gelation on the photophysical properties will be discussed in connection with the formation of the β -phase upon gelation.

Experimental Section

Preparations of Solutions and Gels. Poly(9,9-dioctylfluorene-2,7-diyl) (PF8) end-capped with dimethyl phthalate was obtained from American Dye Source Inc. The weight-average molecular weight (M_w) was 128 000 g/mol as measured by static light scattering at 25 ± 0.1 °C.¹² The solutions of PF8 and MCH were prepared by stirring their mixtures at ca. 60 °C for 12 h, where macroscopically homogeneous solutions were observed by naked eyes. The PF8/MCH gels were obtained by aging the solutions at 20 °C for sufficiently long time.

Dynamic Light Scattering Measurements. DLS was utilized to probe the gelation process and the thermally induced gel-to-sol transition. The DLS measurements were carried out using an ALV/CGS-3 light scattering spectrometer equipped with an ALV/LSE-5003 multiple- τ digital correlator over the time range 10^{-8} – 10^3 s. The JDS-Uniphase solid-state He–Ne laser having the output power of ca. 22 mW at the operating wavelength of 632.8 nm was used as the light source. In this study, the autocorrelation function of the light scattering intensity, $G(q,t) = \langle I(q,t)I(q,0) \rangle / \langle I(q,0) \rangle^2$, with $I(q,0)$ being the mean light scattering intensity at a scattering vector q was measured. The measured normalized electric correlation function $g^{(1)}(t)$ was obtained from the linear fit model:

$$g^{(1)}(t) = \int_{\tau_{\min}}^{\tau_{\max}} e^{-\tau t} G(q, \tau) d\tau \quad (1)$$

The measured normalized intensity correlation function $g^{(2)}(t)$ is related to $g^{(1)}(t)$ through the Siegert relation.^{20,21}

$$g^{(2)}(t) = 1 + \beta |g^{(1)}(t)|^2 \quad (2)$$

When the solution forms the large-scale heterogeneity or gels, the data analysis fits an integral type model function to the correlation function using a constrained regularization method. For DLS data, the mathematical background of regularization is described in great detail for the CONTIN 2DP program by Provencher.²²

$$g^{(2)}(t) = 1 + \beta \left| a_1 \exp(-a_2 \tau) + \sum_{i=1}^j \frac{a_{2i+1}}{1 + a_{2i+1} \tau} \right|^2 \quad j = 1, 2 \quad (3)$$

For a system exhibiting a distribution of collective motions, $g^{(1)}(t)$ can be represented by the superposition of exponential decay functions. Laplace inversion routine of $g^{(1)}(t)$ was performed to yield the distribution of decay times $A(\tau)$, viz.

$$g^{(1)}(t) = \int_0^\infty A(\tau) \exp(-t/\tau) d\tau \quad (4)$$

Small-Angle X-ray Scattering (SAXS) Measurements. The SAXS experiments were mainly performed at the National Synchrotron Radiation Research Center (NSRRC) 17B3 beamline. The energy of the radiation was 8 keV, and its corresponding wavelength was 1.55 Å; a two-dimensional Mar charge-coupled device (CCD) detector with 512×512 pixel resolution was used to collect scattering data. The sample-to-detector distance was ca. 2761.1 mm calibrated by PE standard and silver behenate. The SAXS profiles were corrected for background scattering, sample transmission, empty cell transmission, empty cell scattering, and the background arising from solvent.

Spectral Characterizations. The UV–vis absorption measurements for the $\pi-\pi^*$ and β -phase absorption of PF8 were performed using a Hitachi U-3010 spectrophotometer. The quartz cells of 10 mm thickness were used to measure the spectra of the dilute solutions, while for the semidilute viscous solutions and gels, the samples were sandwiched between two microscope cover glasses to obtain the solution or gel layers of about 100 μ m in thickness. The reported absorbances of the samples have been corrected for the solvent background.

The PL spectra were recorded by using a Perkin-Elmer LS55 spectrophotometer. The samples were placed in sealed glass tubes with the thickness of 1 cm for the measurements. The excitation wavelength was 320 nm. The temperature-dependent experiments were realized by using a thermostat tube heating system.

Polarized Optical Microscopy (POM) Observation. The macrophase separation and the liquid crystalline phase in PF8/MCH gels were observed in real space by a Zeiss Axioskop-40 polarized optical microscope equipped with a Linkam TH600 hot stage. The PF8/MCH solution or gel was inserted between two microscope cover glasses to obtain thin films and then sealed by silicone. To monitor the phase separation, the specimen was equilibrated at 80 °C for 5 min to allow complete dissolution followed by rapid cooling (at ca. 60 °C/min) to 20 °C for phase separation.

Results and Discussion

Dispersion State and Photophysical Properties of PF8 in Freshly Prepared MCH Solutions. The dispersion state of polymer in the solution can be reflected directly from its dynamics. Figure 1 shows the normalized intensity correlation function, $g^2(t) - 1$, and the corresponding decay time distribution $A(\tau)$ (measured at the scattering angle $\theta = 90^\circ$) of freshly prepared PF8/MCH solutions as a function of concentration at 20 °C. For this experiment, the solutions were constantly stirred at 50 °C prior to the DLS measurements; the solutions were then quickly transferred to the sample cells for DLS experiments, and the measurements were completed within 20 min. The solutions in this case were considered as the “unaged system”. Two regimes can be distinguished in Figure 1. Below 0.05 wt %, the intensity correlation function and the decay times corresponding to the maximum $A(\tau)$ do not shift obviously with the increase of concentration. Here the decay time distribution displays a bimodal mode, where the fast mode with the average decay time of about 5 μ s and the intermediate mode with the average decay time of about 0.1 ms are attributed to the motion of the flexible side chains and the translational

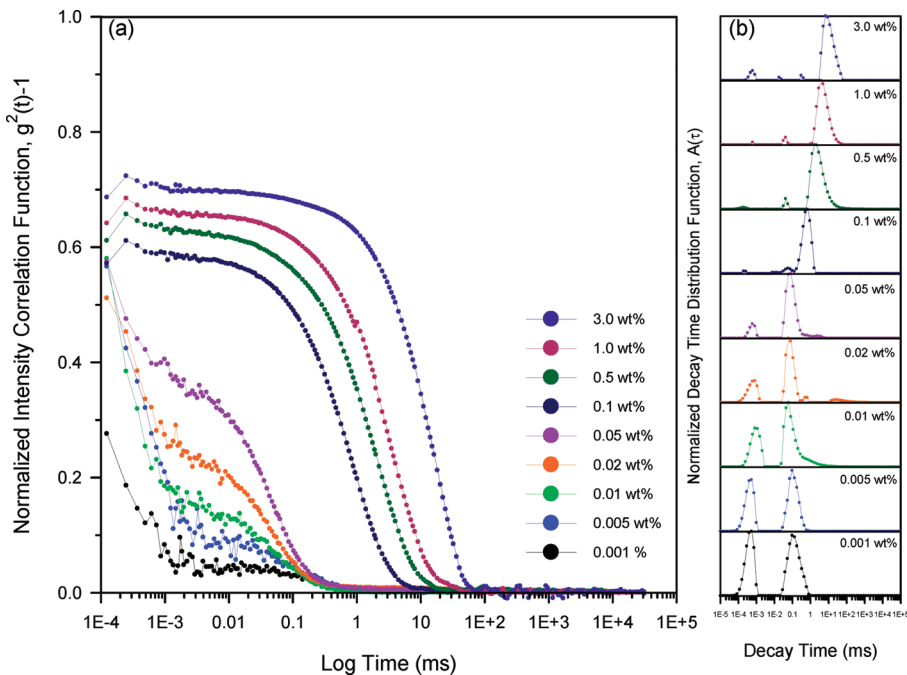


Figure 1. (a) Normalized intensity correlation function, $g^2(t) - 1$ and (b) the decay time distribution $A(\tau)$ of freshly prepared PF8/MCH solutions as a function of concentration at 20 °C (measured at the scattering angle $\theta = 90^\circ$).

diffusion of individual PF8 chains, respectively. The intensity correlation function and $A(\tau)$ exhibit strong concentration dependence when the concentration exceeds 0.05 wt %, where the correlation function grows in intensity and shifts to longer time with increasing concentration. In this case, the average decay time of the slow mode with the average decay time of about 1.0–10 ms is considered as a measure of the dynamics of the aggregates formed by the segmental association of PF8. The fact that the slow mode dominates the relaxation spectra implies that the majority of the PF8 chains form aggregates in the solution.

The critical concentration for the formation of aggregates in the freshly prepared solutions revealed by DLS corroborates well with the emergence of β -phase probed by the UV-vis and PL spectroscopy (see Supporting Information). The mesomorphic β -phase is known to exhibit a characteristic absorption band at 437 nm in the UV spectrum and a series of narrow emission peaks at 470 and 490 nm associated with the 0–2 and 0–3 vibronic replicas, respectively, in the PL spectrum.²³ It was observed from the absorption spectra that the β -phase absorption peak at 437 nm started to appear noticeably at 0.1 wt %, at which the slow mode identified from the DLS measurement also emerged (see Supporting Information). The absorbance of β -phase peak is obviously stronger than that found for PF8/toluene solution at a given concentration,⁹ indicating that the formation of β -phase in freshly prepared solution is greatly promoted by the poorer solvent quality of MCH. The obvious development of β -phase at $c \geq 0.1$ wt % is also manifested by the PL spectra (see Supporting Information), showing that the intensities of the peaks at 418 and 470 nm decrease and grow, respectively, rapidly with increasing concentration.

Gelation Mechanism of PF8/MCH Solution. Gelation is a phase transition from a collection of finite clusters to a state with the formation of an infinite network. The essential feature of a gel is geometrical connections, and hence theoretical works generally emphasize percolation phenomena in the treatment of gelation.^{24–26} It is known that conjugated

polymer solutions undergo physical gelation upon prolonged isothermal aging due to very slow dynamics associated with the structural reorganization.^{8,12} To demonstrate such a slow reorganization, we conduct a time-resolved DLS experiment for 1.0 wt % MCH solution. In this experiment, the freshly prepared solution (prepared at 50 °C) was cooled to 20 °C for isothermal aging. DLS measurement was then conducted continually during the aging process. Figure 2 presents the normalized intensity correlation functions and decay time distributions obtained for different aging times (measured at the scattering angle $\theta = 90^\circ$). The average decay time associated with the slow mode is found to increase with increasing aging time, showing coarsening or clustering of aggregates in the solution upon aging. The originally viscous solution was found to become a gel after 500 min of aging and the corresponding $A(\tau)$ spectrum displays only one single mode, i.e., the slowest mode. The gel thus obtained is visually opaque, which implies the occurrence of phase separation and/or the formation of mesomorphic phase. In a previous study, we found that the gelation of semidilute PF8/toluene solutions was driven mainly by a macrophase separation at subambient temperatures (-20 °C).¹² We proposed that in the course of phase separation the regions enriched with PF8 gradually developed a mesophase composed of sheetlike aggregates. These sheetlike aggregates might increase the viscosity of the PF8-enriched phase, thereby preventing the system from attaining the equilibrium phase-separated morphology by the coarsening process. As a result, the system exhibited an interconnected phase-separated structure that turned the viscous solution into gel.

Such a phase separation process was also identified in the present PF8/MCH solution during the aging process by optical microscopy. The POM micrographs taken at different lengths of aging time (see Supporting Information) showed that the solution is homogeneous at the beginning of the aging process at 20 °C, and domains with birefringent texture due to formation of mesophase gradually develop during aging. The final morphology of the gel thus formed

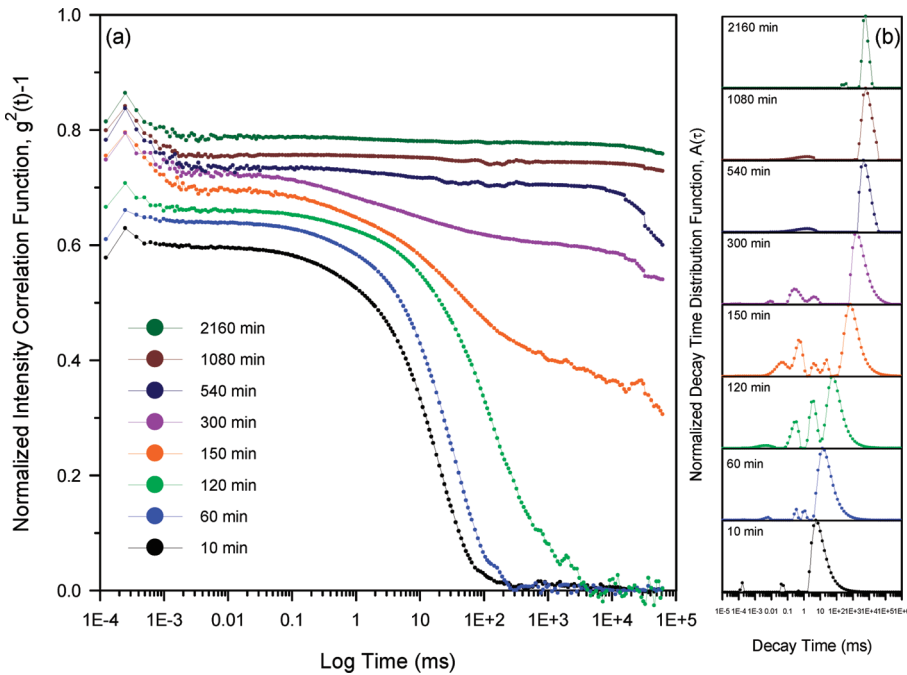


Figure 2. (a) Normalized intensity correlation function, $g^2(t) - 1$, and (b) the decay time distribution $A(\tau)$ of 1.0 wt % PF8/MCH solution obtained after aging at 20 °C for different lengths of time. The scattering angle was 90°.

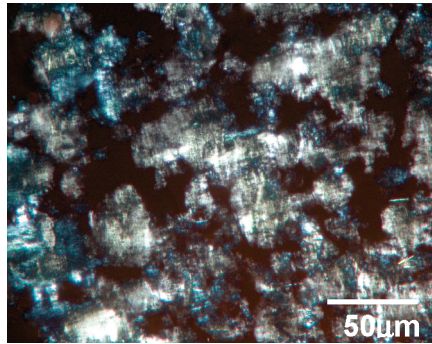


Figure 3. POM micrograph taken after ca. 2000 min of aging to demonstrate the interconnection of the liquid crystalline domains after the phase separation.

presented in Figure 3 reveals the interconnection of liquid crystalline domains. Consequently, the gelation of PF8/MCH solution is also driven by a macrophase separation that occurred in the unstable solution, and the interconnected morphology formed via spinodal decomposition (SD) is arrested due to the formation of mesophase in the PF8-enriched domains.

We have collected the evolution of light scattering intensity in the course of isothermal aging to gain further insight into the phase separation process. Figure 4 shows the double-logarithmic plot of the intensity (measured at the scattering angle of 90°) versus aging time for 0.5 and 1.0 wt % PF8/MCH solutions. The intensities are seen to increase with aging time because of the occurrence of phase separation. The observed sigmoidal curves can be separated into three regions with respect to aging time. Region I corresponds to the induction period of the phase separation, over which the intensity shows no remarkable change with time. The induction time is longer at lower polymer concentration due to a slower phase separation. The scattering intensity in region II increases exponentially with time, as demonstrated from the linearity of the semilog plot

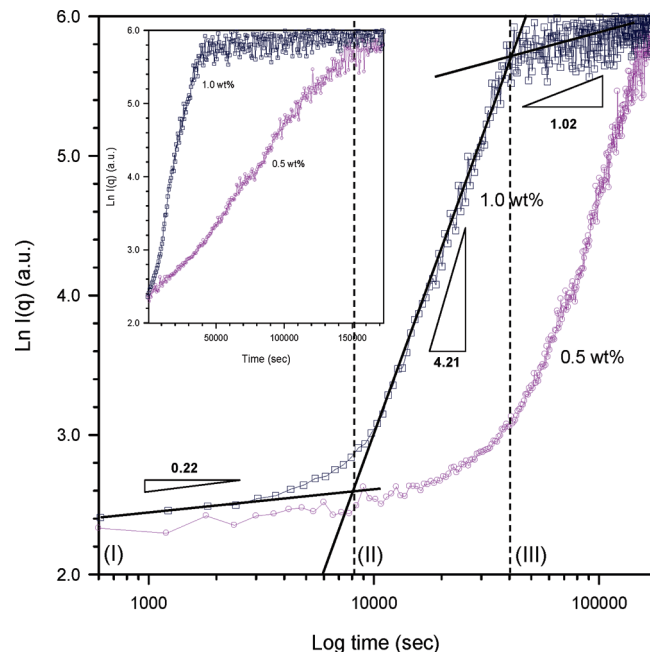


Figure 4. Evolution of light scattering intensity (measured at the scattering angle of 90°) during the aging of 0.5 and 1.0 wt % PF8/MCH solutions at 20 °C. Three regions can be identified for the 1.0 wt % solution. The semilog plot in the inset shows that the time dependence of scattering intensity in region II follows the exponential relationship prescribed by the Cahn–Hilliard theory.

in the inset. Finally, the time dependence of scattering intensity deviates from the exponential relationship in region III. The phase separation behavior in region II is in accord with the Cahn and Hilliard linear theory of SD,²⁷ which prescribes the exponential evolution of scattering intensity as follows:

$$I(q, t) = I(q, t = 0) \exp[2R(q)t] \quad (5)$$

where $I(q,t)$ is the intensity at time t after initiation of SD and $R(q)$ is the growth rate of concentration fluctuation characterized by the wavenumber q and is given by

$$R(q) = D_c q^2 \left[-\frac{\partial^2 f}{\partial c^2} - 2\kappa q^2 \right] \quad (6)$$

where D_c is the translational diffusion coefficient of polymer chains in solution, f is the free energy of mixing, c is the concentration, and κ is the concentration-gradient energy coefficient. According to eq 5, concentration fluctuation growth rate $R(q)$ at a given q can be determined from the slope of the straight line in the plot of $\ln I(q,t)$ vs t . The values of $R(q)$ thus obtained are 3.5 and 14.2×10^{-6} s $^{-1}$ for 0.5 and 1.0 wt % solution, respectively.

The deviation from the exponential relationship in region III is considered to stem from the coarsening effect at the later stage of SD, which has been discussed in many studies.^{28,29} In the later-stage SD, the phase-separated structure coarsens with time, and the nonlinearity in the time evolution of the amplitude of concentration fluctuations becomes increasingly important. The coarsening behavior is characterized by the time evolution of the magnitude of scattering vector $q_m(t)$ at the maximum scattering intensity and the maximum intensity $I_m(t)$. In this case, the intermediate and late stages of SD are characterized by the following scaling laws²⁹

$$I_m(t) \approx t^\beta \quad (7)$$

$$q_m(t) \approx t^{-\alpha} \quad (8)$$

In the intermediate-stage SD, both the amplitude and the wavelength of concentration fluctuations increase with time. On the other hand, the interfaces between two coexisting phases are well developed in the late-stage SD, and the local concentration of each component in the domains reaches its equilibrium value. Although the amplitude of the concentration fluctuation has reached the equilibrium values, the domain sizes are still growing to reduce the interfacial free energy. Consequently, the scaling exponents α and β in the intermediate stage exhibit the relationship of²⁹

$$\beta/\alpha > 3 \quad (9)$$

while the relationship changes into

$$\beta/\alpha = 3 \quad (10)$$

for the late stage. This change of scaling exponent would allow one to distinguish between these two stages.

Figure 5 presents the time evolution of the light scattering spectrum ($I(q)$ vs q) of 1.0 wt % PF8/MCH solution at 20 °C. The primary peak is observable at 100 min, and it grows in intensity as the aging progresses. The position of this peak remains largely unperturbed up to 150 min, but it shifts to lower q with increasing aging time afterward. Interestingly, at least one more scattering peak is discernible besides the primary peak. In polystyrene/poly(butyl methacrylate) blend, double scattering peaks had been observed during SD, which suggested that a second or an alternative relaxation mechanism dominating the coarsening process.³⁰ The additional peaks observed here may be attributed to the local heterogeneity in the PF8-enriched domains. As PF8 is able to form liquid crystalline and crystalline structure, it is likely that the nanoscale liquid crystalline entity (e.g., the sheetlike aggregates) and crystalline entity further assemble to form larger superstructures within these domains

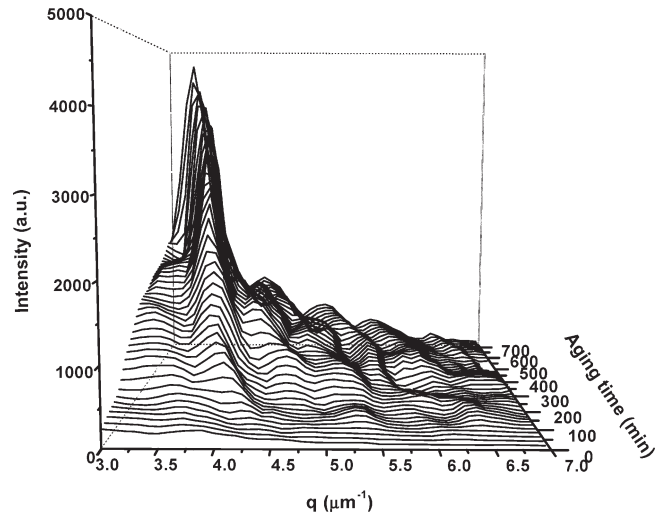


Figure 5. Time evolution of the light scattering profile ($J(q)$ vs q) during the aging of 1.0 wt % PF8/MCH solution at 20 °C. The scattering pattern is seen to exhibit multiple peaks, which may be due to the heterogeneity in the PF8-enriched domains.

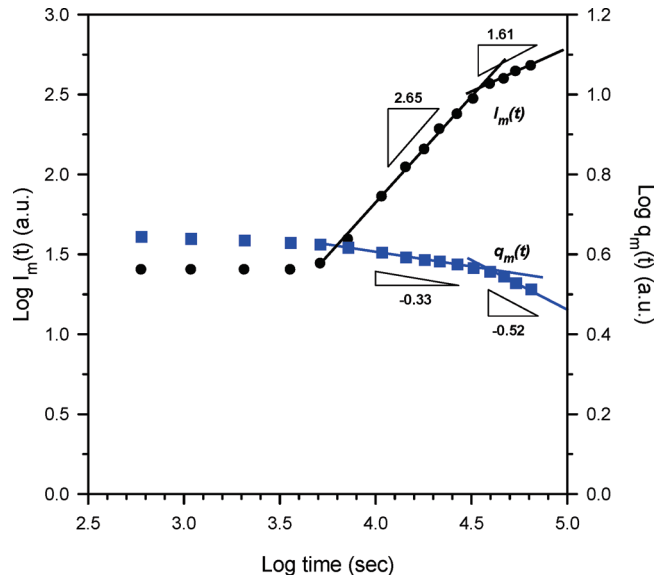


Figure 6. Power-law dependence of $q_m(t)$ and $I_m(t)$ on time of 1.0 wt % PF8/MCH solution. The data of $I_m(t)$ and $q_m(t)$ were associated with the primary peak in Figure 5. The slopes observed in the plot allow us to identify the intermediate and late stage of SD in the phase separation process.

(e.g., the formation of the network of the sheetlike aggregates¹⁹), and the presences of these superstructures give rise to other length scales of concentration fluctuations leading to multiple scattering peaks.

Figure 6 shows the variations of $q_m(t)$ and $I_m(t)$ of the primary peak with aging time in double-logarithmic scale. The slopes of $I_m(t)$ and of $q_m(t)$ at 150 min < t < 600 min are 2.65 and -0.33 , respectively, while those at $t > 600$ min are 1.61 and -0.52 , respectively. The corresponding ratios of β/α are hence ca. 8 and 3, which corresponds to the intermediate and late stage of SD, respectively, based on the criteria prescribed by eqs 9 and 10.

The effect of gelation on the optical spectra is demonstrated in Figure 7 showing the UV-vis and PL spectra collected at different lengths of aging times for 1.0 wt % PF8/MCH solution. It can be observed from the absorption spectra that the β -phase absorption peak at 437 nm grows

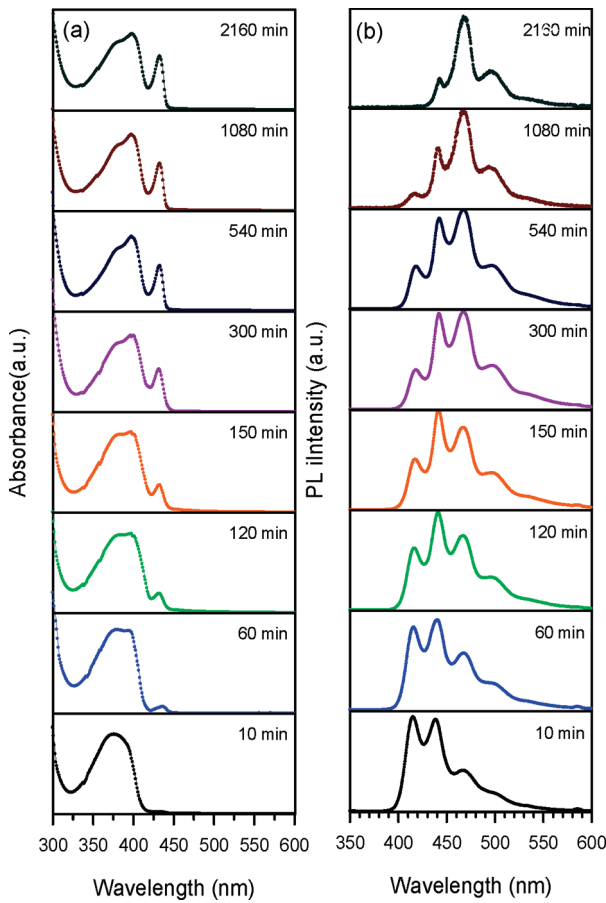


Figure 7. (a) UV-vis spectra and (b) PL spectra of 1.0 wt % PF8/MCH solution taken at different aging times at 20 °C. The absorption peak at 437 nm and emission peaks at 470 and 495 nm grow with increasing aging time, indicating the development of β -phase during aging.

with increasing aging time. It is noted that an additional absorption peak at 400 nm also emerges, and its absorbance increases with increasing aging time. The presence of this peak has been attributed to the formation of C_α or C_γ conformational isomers^{16,31} or the transformation of the randomly twisted local PF backbone motifs into a highly ordered PF backbone motif (a $P\text{-}5_2$ helix) and other unclear local backbone motifs.³²

The PL spectra also change significantly with aging time, where the intensities of the emission peaks at 418 and 440 nm decrease remarkably, while the emission peaks at 470 and 495 nm grow progressively with increasing aging time. The observed variation of the spectral features with aging attests that gelation of PF8/MCH solution is accompanied by the formation of β -phase. This is in parallel with the gelation behavior of PF8/toluene system reported previously.¹²

The increase of the relative volume fraction of β -phase during the aging process is evaluated from the growth of the intensity of 470 nm peak ($I_{470\text{nm}}$) in the PL spectra as well as the absorbance of the UV absorption peak at 437 nm ($A_{437\text{nm}}$). In this case, the relative volume fraction at a given time t is calculated by

$$f_\beta(t) = \frac{I_{470\text{nm}}(t) - I_{470\text{nm}}(0)}{I_{470\text{nm}}(2160 \text{ min}) - I_{470\text{nm}}(0)} \quad (11)$$

$$f_\beta(t) = \frac{A_{437\text{nm}}(t) - A_{437\text{nm}}(0)}{A_{437\text{nm}}(2160 \text{ min}) - A_{437\text{nm}}(0)} \quad (12)$$

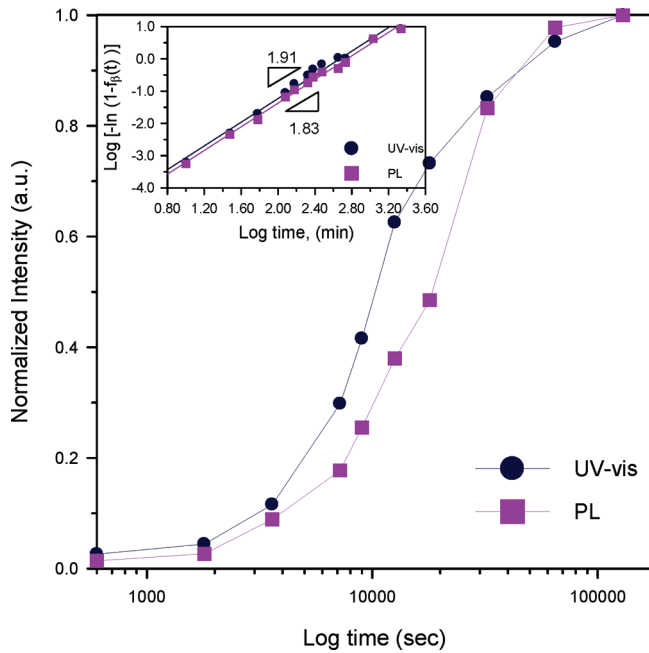


Figure 8. Temporal development of the β -phase during aging deduced from the optical spectra in Figure 7. The inset shows the corresponding Avrami plots, from which the growth of the β -phase is found to be two-dimensional.

The relative volume fractions thus calculated are plotted against aging time in Figure 8. It can be seen that the development of β -phase also displays sigmoidal curve. We assume that the formation of β -phase follows the nucleation and growth mechanism, and then the temporal variation of the volume fraction may be described by the classical Avrami equation^{33,34}

$$f_\beta(t) = 1 - \exp(-k_\beta t^n) \quad (13)$$

where k_β is the overall rate constant depending on the nucleation and growth rate and n is the Avrami exponent determined by the dimensionality of growth and the nucleation mechanism. The Avrami plot, i.e., $\log\{-\ln[1 - f_\beta(t)]\}$ vs $\log t$, is displayed in the inset Figure 8. The value of n obtained using $f_\beta(t)$ derived from UV-vis and PL spectra are ca. 1.91 and 1.83, respectively. The close proximity of n to the value of 2.0 signals a two-dimensional growth of the β -phase; therefore, the basic morphological entity of the β -phase should be sheet or disklike, as has been pointed out by Knaapila et al.¹⁹ The presence of these sheetlike objects is verified by the SAXS profile of PF8/MCH gel obtained after sufficient aging, where the SAXS intensity in the intermediate- q region follows q^{-2} power-law dependence, and the entire profile can be fitted by the form factor of randomly oriented disks with thickness of ca. $23 \pm 2 \text{ \AA}$.

Our results have hence revealed that the gelation of PF8/MCH solution is driven by a macrophase separation proceeding through spinodal decomposition. During the phase separation, a mesophase composing at least a fraction of β -phase forms in the regions enriched of PF8. The sheetlike aggregates associated with the β -phase might further assemble to form larger superstructures within these domains (e.g., the formation of network of the sheetlike aggregates¹⁹), and the presence of these superstructures increases the viscosity of the PF8-enriched phase, such that the interconnected morphology formed through SD is arrested, leading to gelation of the system.

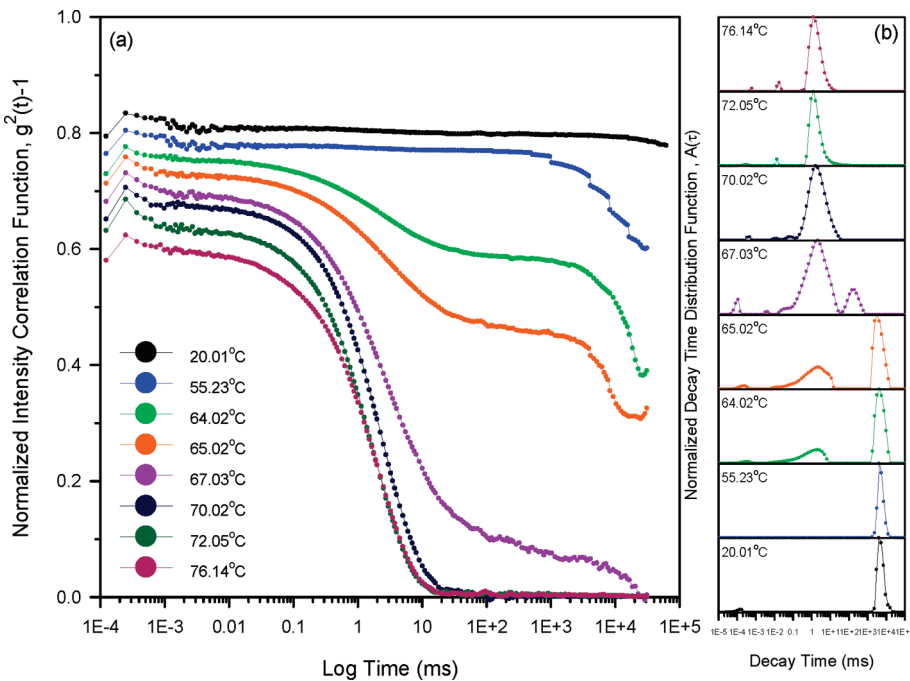


Figure 9. (a) Normalized intensity correlation function, $g^2(t) - 1$, and (b) decay time distribution, $A(\tau)$, of 1.0 wt % PF8/MCH gel measured in the heating cycle with a heating rate of 0.5 °C/min.

Thermally Induced Gel-to-Sol Transition. The PF8/MCH gel formed via isothermal aging can be disrupted and transformed into liquid solution by moderate heating because of the improvement of solvent quality of MCH to PF8. Figure 9 displays the temperature dependences of normalized intensity correlation function and decay time distribution of 1.0 wt % PF8/MCH gel measured in a heating cycle. Below ca. 65 °C where the system is apparently in the gel state, the decay of the correlation function occurs at very long time, and the corresponding $A(\tau)$ spectrum displays only the slowest mode with very large average decay time (at ca. 6×10^3 ms). As the gel-to-sol transition is approached (ca. 67–70 °C), the correlation function profile changes remarkably and the slow mode and the intermediate mode appear in the $A(\tau)$ spectrum. Above 70 °C, the correlation function and $A(\tau)$ indicate a well-mixed PF8/MCH solution. Figure 10 presents the temperature-dependent scattering intensity (measured at the scattering angle of 90° by DLS) of the PF8/MCH gels (with the concentration ranging from 0.1 to 3.0 wt %) obtained in a heating cycle. The scattering intensity exhibits an abrupt drop across the gel-to-sol transition, which indicates that the transition is a first-order transition. It is interesting to note that the gel-to-sol transition temperature increases with increasing polymer concentration. The observed gel-to-sol transition has a direct relevance with the dissipation of the sheetlike aggregates and may be related to the membrane–isotropic transition temperature (T_{mem}^*) defined by the Knaapila et al.¹⁹ Figure 11 shows the temperature-dependent SAXS profiles in double-logarithmic plot obtained by heating the 1.0 wt % gel. A change of the slope from -2 to -1 can be observed upon heating to 71.6 °C, showing that the sheetlike objects are disrupted and the stiff PF8 chains redissolve into the solvent to dominate the SAXS profile.

The influence of the thermally induced gel-to-sol transition on the photoemission behavior is evaluated from the temperature-dependent PL experiment, where the PL spectra were collected *in situ* in a heating cycle with the heating rate of 1.0 °C/min. Figure 12 displays the temperature-dependent

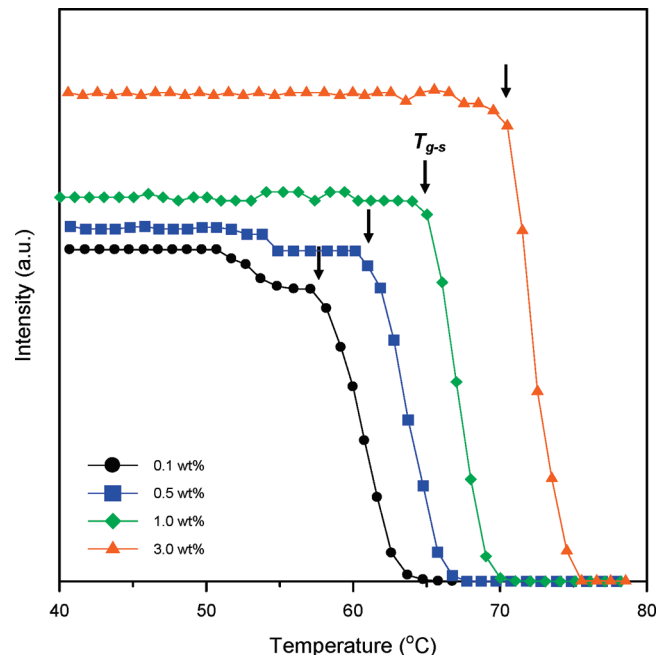


Figure 10. Scattering intensity of PF8/MCH gels (formed from 0.1 to 3.0 wt % solutions) as a function of temperature in a heating cycle. The intensities undergo an abrupt drop across the gel-to-sol transition.

PL spectra of 1.0 wt % PF8/MCH gel. It can be seen that the emission intensities at 470 and 495 nm decrease remarkably, while those at 418 and 440 nm increase progressively as the temperature is increased due to the disruption of β -phase. The drop of the intensities of 470 and 495 nm peaks is the most drastic when the temperature is raised from 65 to 70 °C (i.e., across the gel-to-sol transition temperature). The results of light scattering, SAXS and PL spectra thus reveal that the gel-to-sol transition is accompanied by the homogenization of the solution and the dissociation of the sheetlike aggregates as well as the β -phase.

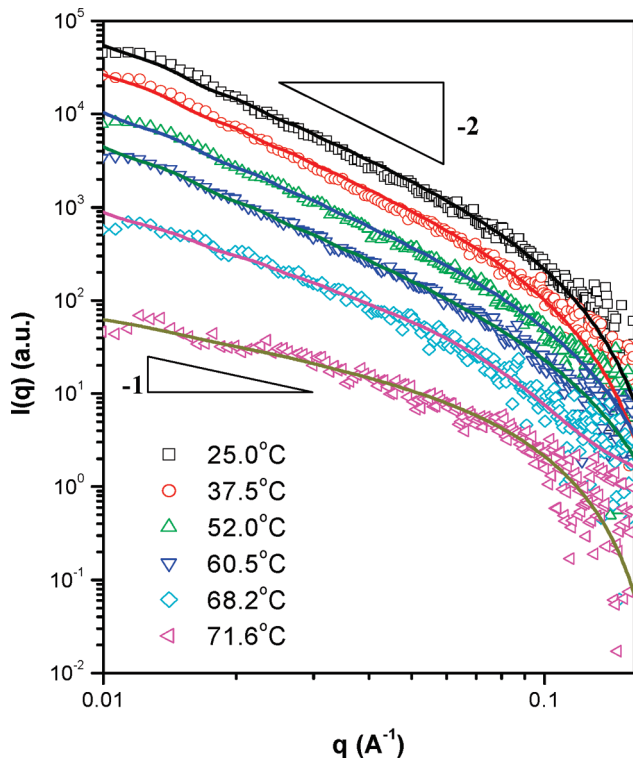


Figure 11. Temperature-dependent SAXS profiles of 1.0 wt % PF8/MCH gels collected in a heating cycle. Below 60.5 °C, the scattering intensities at low- q displays q^{-2} dependence, suggesting the existence of sheetlike aggregates. The power-law dependence transforms to q^{-1} at 71.6 °C due to the disruption of the sheetlike aggregates and the stiff PF8 chains redissolve into the solvent to dominate the SAXS profile.

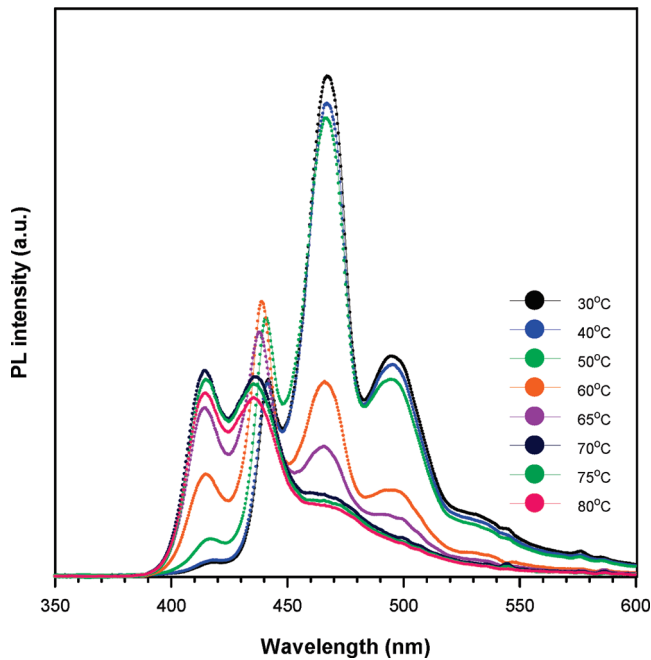


Figure 12. Temperature-dependent PL spectra of 1.0 wt % PF8/MCH gel. It can be seen that the emission intensities at 470 and 495 nm decrease while those at 418 and 440 nm increase with increasing temperature.

Conclusions

When the originally homogeneous PF8/MCH solution was aged under ambient conditions, the viscous solution turned into a gel with high viscosity. Here we have shown that the gelation was

driven by a phase separation occurred through the spinodal decomposition mechanism, where the interconnected morphology arrested during the phase separation led to gelation. In contrast to the conventional liquid–liquid phase separation, the macrophase separation in the present system yielded the coexistence of an isotropic liquid phase and a liquid crystalline phase. Local heterogeneity may be present in the liquid crystalline domains so as to give rise to multiple modes of concentration fluctuations. The aging also induced the development of β -phase in the polymer-enriched phase proceeding through two-dimensional growth, and the β -phase dominated the photoemission spectra due to energy transfer effect. The gel transformed into a transparent liquid upon heating and the dissolution temperature detected by light scattering agreed with the melting temperature of β -phase. It is noted that the presence of β -phase in the PF8 film is often desirable for light-emitting diode application as this structure can promote color stability under different driving voltages compared with amorphous phase.³⁵ The present study has demonstrated that the formation of β -phase in PF8/MCH solution could be promoted by room-temperature aging; therefore, one may expect that the film with higher amount of β -phase may be obtained if it is cast from the aged solution or gel. This was indeed observed, as the wide-angle X-ray scattering profile of the film cast from PF8/MCH gel exhibited an obviously stronger β -phase (200) diffraction peak than that of the film cast from the freshly prepared solution irrespective of the rate of solvent removal (see Supporting Information). The result also demonstrated the crucial role of solution structure on the film morphology formation of conjugated polymers.

Acknowledgment. We acknowledge the financial supports of the National Science Council of the Republic of China under Grants NSC 98-2221-E-168-002 and NSC 97-2752-E-002-PAE.

Supporting Information Available: UV-vis and PL spectra of freshly-prepared PF8/MCH solutions (Figure S1), a series of POM micrographs of PF8/MCH 1.0 wt % solution (Figure S2), and wide-angle X-ray scattering profiles of the PF8 films (Figure S3). This material is available free of charge via the Internet at <http://pubs.acs.org>.

References and Notes

- (a) Burroughes, J. H.; Bradley, D. D. C.; Brown, A. R.; Marks, R. N.; Mackay, K.; Friend, R. H.; Burns, P. L.; Holmes, A. B. *Nature (London)* **1990**, *347*, 539–541. (b) Gross, M.; Müller, D. C.; Nothofer, H.-G.; Scherf, U.; Neher, D.; Bräuchle, C.; Meerholz, K. *Nature (London)* **2000**, *405*, 661–665.
- Hoppe, H.; Sariciftci, N. S. *J. Mater. Res.* **2004**, *19*, 1924–1945.
- Sirringhaus, H.; Brown, P. J.; Friend, R. H.; Nielsen, M. M.; Bechgaard, K.; Langeveld-Voss, B. M. W.; Spiering, A. J. H.; Janssen, R. A. J.; Meijer, E. W.; Herwig, P.; de Leeuw, D. M. *Nature* **1999**, *401*, 685–688.
- Nguyen, T.-Q.; Doan, V.; Schwartz, B. J. *J. Chem. Phys.* **1999**, *110*, 4068–4078.
- Nguyen, T.-Q.; Martini, I. B.; Liu, J.; Schwartz, B. J. *J. Phys. Chem. B* **2000**, *104*, 237–255.
- Ou-Yang, W. C.; Chang, C. S.; Chen, H. L.; Tsao, C. S.; Peng, K. Y.; Chen, S. A.; Han, C. C. *Phys. Rev. E* **2005**, *72*, 031802.
- Li, Y. C.; Chen, C. Y.; Chang, Y. X.; Chuang, P. Y.; Chen, J. H.; Chen, H. L.; Hsu, C. S.; Ivanov, V. A.; Khalatur, P. G.; Chen, S. A. *Langmuir* **2009**, *25*, 4668–4677.
- Li, Y. C.; Chen, K. B.; Chen, H. L.; Hsu, C. S.; Tsao, C. S.; Chen, J. H.; Chen, S. A. *Langmuir* **2006**, *22*, 11009–11015.
- Knaapila, M.; Garamus, V. M.; Dias, F. B.; Almásy, L.; Galbrecht, F.; Charas, A.; Morgado, J.; Burrows, H. D.; Scherf, U.; Monkman, A. P. *Macromolecules* **2006**, *39*, 6505–6512.
- Huang, W. Y.; Matsuoka, S.; Kwei, T. K.; Okamoto, Y. *Macromolecules* **2001**, *34*, 7166–7171.
- Wang, P. S.; Lu, H. H.; Liu, C. Y.; Chen, S. A. *Macromolecules* **2008**, *41*, 6500–6504.

- (12) Chen, J. H.; Chang, C. S.; Chang, Y. X.; Chen, C. Y.; Chen, H. L.; Chen, S. A. *Macromolecules* **2009**, *42*, 1306–1314.
- (13) Malik, S.; Jana, T.; Nandi, A. K. *Macromolecules* **2001**, *34*, 275–282.
- (14) Bliznyuk, V. N.; Carter, S. A.; Scott, J. C.; Klärner, G.; Miller, R. D.; Miller, D. C. *Macromolecules* **1999**, *32*, 361–369.
- (15) Rahman, M. H.; Chen, C. Y.; Liao, S. C.; Chen, H. L.; Tsao, C. S.; Chen, J. H.; Liao, J. L.; Ivanov, V. A.; Chen, S. A. *Macromolecules* **2007**, *40*, 6572–6578.
- (16) Chunwaschirasiri, W.; Tanto, B.; Huber, D. L.; Winokur, M. J. *Phys. Rev. Lett.* **2005**, *94*, 107402 (1–4).
- (17) Rothe, C.; King, S. M.; Dias, F.; Monkman, A. P. *Phys. Rev. B* **2004**, *70*, 195213.
- (18) Kitts, C. C.; Vanden Bout, D. A. *Polymer* **2007**, *48*, 2322–2330.
- (19) Knaapila, M.; Stepanyan, R.; Torkkeli, M.; Garamus, V. M.; Galbrecht, F.; Nehls, B. S.; Preis, E.; Scherf, U.; Monkman, A. P. *Phys. Rev. E* **2008**, *77*, 051803.
- (20) Schmitz, K. S. *An Introduction to Dynamic Light Scattering by Macromolecules*; Academic Press: New York, 1990.
- (21) Brown, W. *Dynamic Light Scattering*; Clarendon Press: Oxford, 1993.
- (22) (a) Provencher, S. W. *Comput. Phys. Commun.* **1982**, *27*, 213–227.
(b) Provencher, S. W. *Comput. Phys. Commun.* **1982**, *27*, 229–242.
- (23) Moynihan, S.; Iacopino, D.; O'Carroll, D.; Lovera, P.; Redmond, G. *Chem. Mater.* **2008**, *20*, 996–1003.
- (24) Chou, C. M.; Hong, P. D. *Macromolecules* **2003**, *36*, 7331–7337.
- (25) Chou, C. M.; Hong, P. D. *Macromolecules* **2004**, *37*, 5596–5606.
- (26) Chou, C. M.; Hong, P. D. *Macromolecules* **2008**, *41*, 6540–6545.
- (27) Cahn, J. W.; Hilliard, J. E. *J. Chem. Phys.* **1958**, *28*, 258–267.
- (28) Langer, J. S.; Bar-on, M.; Miller, H. D. *Phys. Rev. A* **1975**, *11*, 1417–1429.
- (29) Hashimoto, T.; Itakura, M.; Shimidzu, N. *J. Chem. Phys.* **1986**, *85*, 6773–6786.
- (30) He, M. J.; Liu, Y. M.; Yi, F.; Ming, J.; Han, C. C. *Macromolecules* **1991**, *24*, 464–473.
- (31) Knaapila, M.; Dias, F. B.; Garamus, V. M.; Almásy, L.; Torkkeli, M.; Leppänen, K.; Galbrecht, F.; Preis, E.; Burrows, H. D.; Scherf, U.; Monkman, A. P. *Macromolecules* **2007**, *40*, 9398–9405.
- (32) Tang, H. Z.; Fujiki, M.; Sato, T. *Macromolecules* **2002**, *35*, 6439–6445.
- (33) Avrami, M. *J. Chem. Phys.* **1939**, *7*, 1103–1112.
- (34) Avrami, M. *J. Chem. Phys.* **1941**, *9*, 177–184.
- (35) Morgado, J.; Alcácer, L.; Charas, A. *Appl. Phys. Lett.* **2007**, *90*, 201110.